Dalton Transactions

Accepted Manuscript

ROYAL SOCIETY OF CHEMISTRY

www.rsc.org/dalton

Dalton Transactions

RSCPublishing

ARTICLE

Synthesis of the Phase Pure $Ba_3Si_6O_{12}N_2:Eu^{2+}$ Green Phosphor and its Application in High Color Rendition White LEDs

Wanyuan Li,[a, b] Rong-Jun Xie,[a, c, †] Tianliang Zhou,[a] Lihong Liu,[c] Yuejin Zhu[b]

Cite this: DOI: 10.1039/x0xx00000x

Received 00th January 2012,
Accepted 00th January 2012

DOI: 10.1039/x0xx00000x

www.rsc.org/

Abstract

The promising green oxynitride phosphor, $Ba_3Si_6O_{12}N_2:Eu^{2+}$, was synthesized at 1350 °C for 5 hours in a reducing N_2/H_2 (5%) atmosphere by using the solid-state reaction method. The phase purity was investigated by varying the nominal compositions, and the pure phase was achieved by carefully controlling the Si/Ba and O/Ba ratios. The phosphor displayed a broad excitation band covering from the ultraviolet (UV) to the blue spectral region, and showed a single symmetrical emission band peaking at 525 nm with a full width at half maximum (FWHM) of ~ 68 nm. The as-prepared green phosphor exhibited a small thermal quenching, remaining 90% of the initial emission intensity when measured at 200 °C. The internal and external quantum efficiencies measured under the 450 nm excitation were 68 and 38%, respectively. Color temperature-tunable white LEDs with high color rendering index of Ra = 88-94 were attained by combining the prepared green phosphor and a red phosphor $Sr_2Si_5N_8:Eu^{2+}$ with a blue LED chip.

1. Introduction

White light-emitting diodes (LEDs) are considered as next generation solid state lighting sources due to their high efficiency, long lifetime, robustness and environment friendly[1]. Phosphor is one of key components in these devices. White LEDs, commercialized in 1996, are commonly fabricated by combining a blue GaInN LEDs with a yellow $(Y, Gd)_3(Al, Ga)_5O_{12}:Ce^{3+}$ (YAG:Ce) phosphor[2]. The YAG:Ce phosphor shows a high luminescence efficiency and chemical stability. However, it is lack of enough red components in its spectrum, making the white LEDs only has a medium color rendering index (Ra < 80)[3, 4]. To attain high color rendition white LEDs (Ra > 80), highly efficient green and red phosphors are generally required. Recently, rare earth-activated nitride/oxynitride luminescent materials have attracted much attention because of their excellent photoluminescent properties for white LEDs applications, which include Eu^{2+}-doped red $M_2Si_5N_8$ (M = Ba, Sr and Ca)[5-7] and $CaAlSiN_3$ [8] phosphors, green β-SiAlON[9-11], $MSi_2O_2N_2$ (M = Ba, Sr, Ca)[12-15] and $Sr_5Al_{5+x}Si_{21-x}N_{35-x}O_{2+x}$ ($x \approx 0$)[16] phosphors, and yellow α-SiAlONs[17, 18], as well as Ce^{3+}-activated yellow $CaAlSiN_3$[19], $Y_3Si_6N_{11}$[20], $La_3Si_6N_{11}$[21, 22] and $SrAlSi_4N_7$[23, 24] phosphors. β-SiAlON:Eu^{2+} is a very promising green phosphor that has a narrow emission band (FWHM = 55 nm), which enables it to be widely used in wide color gamut white LED backlights and high color rendition general lighting. However, the synthesis of β-SiAlON:Eu^{2+} usually requires very high temperature (1800-2000 °C) and high gas pressure (> 1.0 MPa). Therefore, from the viewpoint of production cost it is very meaningful to find green-emitting oxynitride phosphors that can be synthesized at ambient conditions.

A number of highly efficient green phosphors, including orthosilicate ($Sr_2SiO_4:Eu^{2+}$, $Ba_2SiO_4:Eu^{2+}$)[25, 26], thiogallate ($MGa_2S_4:Eu^{2+}$, M=Ca, Sr, Ba)[27] and yttrium aluminum garnet ($Y_3Al_5O_{12}:Ce^{3+}$)[28], have been developed for use in white LEDs. On the other hand, these phosphors (except $Y_3Al_5O_{12}:Ce^{3+}$) are suffering from large thermal quenching and serious moisture sensitivity, making them hard to be used in highly reliable white LEDs. Recently, europium doped green phosphors in the system of $Ba_3Si_6O_xN_y:Eu^{2+}$ with (x,y) = (6,6), (9,4), (12,2), (15,0) have attracted great attention due to the easy synthesis, high thermal quenching temperature (except $Ba_3Si_6O_9N_4$), and high quantum efficiency[29-32]. Among these, $BaSi_2O_2N_2:Eu^{2+}$ (= $Ba_3Si_6O_6N_6:Eu^{2+}$) has been extensively investigated in terms of its structure, photoluminescence as well as mechanoluminescence[12, 32-34]. Differing from other counterparts, $Ba_3Si_6O_9N_4:Eu^{2+}$ exhibits strong thermal quenching and a low luminescence efficiency at room

temperature[29, 35]. The reason, suggested by Mikami et al., is that the lowest 5d states of Eu^{2+} are very close to the conduction bands of $Ba_3Si_6O_9N_4$, and thermally-activated photoionization occurs at room temperature. On the other hand, although it has a similar crystal structure with $Ba_3Si_6O_9N_4$,[36] $Ba_3Si_6O_{12}N_2:Eu^{2+}$ shows smaller thermal quenching and higher luminance[29]. Furthermore, it exhibits a narrow emission band and high color purity, which has the comparable photoluminescent properties to β-SiAlON:Eu^{2+}, and is thus potentially used for wide color gamut white LEDs.

The synthesis of $Ba_3Si_6O_{12}N_2:Eu^{2+}$ often encounters problems of phase purity[37-39] with orthosilicates formed as impurity phases that significantly decrease the thermal stability of the green phosphor. To achieve phase pure $Ba_3Si_6O_{12}N_2:Eu^{2+}$, some special synthetic methods have been employed, for instance, high-temperature/high-pressure synthesis[30] as well as using the $Ba_3SiO_5:Eu^{2+}$ precursor[40]. However, these approaches are involved with either complicated facilities or multi-step processing. In this work, we attempted to obtain the high purity $Ba_3Si_6O_{12}N_2:Eu^{2+}$ phosphor by simply controlling the Si/Ba and O/Ba ratios of the starting powders *via* the conventional solid state reaction method. The photoluminescent properties of the prepared phosphor were investigated in terms of photoluminescence spectra, quantum efficiency and thermal quenching. Finally, the application of the green phosphor to high color rendition white LEDs was demonstrated.

2. Experimental section

$Ba_3Si_6O_{12}N_2:Eu^{2+}$ green phosphors were synthesized by using starting powders of $BaCO_3$ (Aladdin, AR), SiO_2 (Aladdin, >99%), Si_3N_4 (UBE E-10, >96%), and Eu_2O_3 (BAOTOU STEEL RARE-EARTH, >99%). The weighted raw powders were mixed in a mortar by hand and packed into the BN crucibles, and then fired in a tube furnace under a reducing atmosphere N_2/H_2 (5%). The powders were firstly heated to 900 ^oC at a heating rate of 10 ^oC min^{-1}, and then to 1350 ^oC at a rate of 6 ^oC min^{-1}. The holding time for all samples was 5 hours. After firing, the samples were cooled down to room temperature in the furnace.

The phase purity of $Ba_{3-x}Eu_xSi_6O_{12}N_2$ (x=0.05~0.3) was analyzed by X-ray powder diffraction (XRD, Advance D8, Bruker, Cu K_α, λ=1.5418 Å), operating at 40 KV and 40 mA in the 2θ range of 10 ^{o} – 70 ^{o} with a step size of 0.02 ^{o} and 0.2 s per step. Photoluminescence spectra were measured at room temperature on a fluorescent spectrophotometer (F-4600, Hitachi) with a 200W Xe-lamp as an excitation source. The thermal quenching was evaluated at the temperature range of 30-350 ^oC by using a fluorescence excitation and detection system (Firefly HR4000LED, Ocean Optics). The absorption and quantum efficiency of the prepared phosphor were measured using a Hamamatsu MPCD-7000 multichannel photo detector with a 200 W Xe-lamp as an excitation and the reflection spectrum of $BaSiO_4$ white standards was used for calibration. The morphology of $Ba_3Si_6O_{12}N_2:Eu^{2+}$ was observed by scanning electron microscopy (FE-SEM, S-4800, Hitachi). To fabricate white LEDs, the prepared $Ba_3Si_6O_{12}N_2:Eu^{2+}$ green phosphor was mixed with a commercial $Sr_2Si_5N_8:Eu^{2+}$ red phosphor and epoxy, and the phosphor blend was then mounted on a blue LED chip (460 nm). The optical properties of white LEDs were investigated by a high accuracy array spectroradiometer (Haas-2000, Everfine) under forward-bias current of 20 mA at room temperature.

3. Results and discussion

3.1. Phase identification and microstructure

The target phosphor $Ba_3Si_6O_{12}N_2:Eu^{2+}$ was prepared under the flowing N_2 - H_2 (5%) atmosphere through the following chemical reaction:

$$6BaCO_3+9SiO_2+Si_3N_4 \xrightarrow[Eu_2O_3]{1350^oC,\ H_2/N_2} 2Ba_3Si_6O_{12}N_2:Eu^{2+}+6CO_2 \quad (1)$$

The XRD patterns of the samples with different Si/Ba ratios in the starting powders are given in Fig. 1. As seen, the sample with Si/Ba = 2.00, which was stoichiometrically weight out, revealed that most of the high intensity peaks match well with the reported data of Mikami et al.[29]. It indicates that the $Ba_3Si_6O_{12}N_2$ phase was dominated. In addition, some weak diffraction peaks of impurities were detected, which can be identified as orthorhombic $BaSi_2O_5$ and monoclinic $Ba_5Si_8O_{21}$. Similar to $Ba_3Si_6O_{12}N_2$ consisting of corner sharing [SiO_3N] tetrahedra, both barium orthosilicates were structurally formed by corner-sharing [SiO_4] tetrahedra, as shown in Fig. 2. By considering the formation temperature of barium orthosilicate[31], one can suppose that the $Ba_3Si_6O_{12}N_2$ phase forms via the dissolution-diffusion-precipitation stages: (i) the low-melting-point barium orthosilicates firstly emerge when the temperature is up to about 1000 – 1200 ^oC; (ii) when the temperature further rises to ~ 1350 ^oC, Si_3N_4 starts to dissolve in the Ba-Si-O liquid phase; (iii) the target phase $Ba_3Si_6O_{12}N_2$ then precipitates from the nitrogen saturated liquid phase accompanying with the formation of barium orthosilicates .

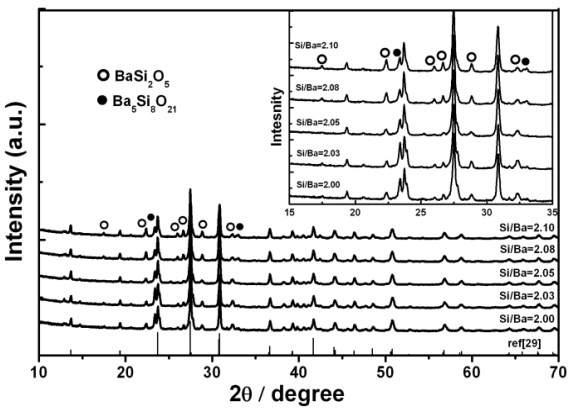

Fig. 1 X-ray diffraction patterns of $Ba_{2.85}Eu_{0.15}Si_6O_{12}N_2$ with different ratio of Si/Ba

It is seen that the impurity orthosilicate phases ($BaSi_2O_5$ and $Ba_5Si_8O_{21}$) have the larger O/Ba ratios but smaller (or equal) Si/Ba ratio than $Ba_3Si_6O_{12}N_2$, as shown in Table I. This is indicative of deficiency of Si_3N_4 in the raw materials, caused by the presence of the SiO_2 layer on the partially oxidized Si_3N_4. Therefore, In order to suppress the formation of orthosilicates, the excessive amount of

Si_3N_4 was added, resulting in higher Si/Ba ratios (> 2). As seen in Fig. 1, the amount of both impurity phases reduces with increasing the Si/Ba ratio. Among the two orthosilicates, the content of $Ba_5Si_8O_{21}$ decreases faster than that of $BaSi_2O_5$, implying that the excessive Si_3N_4 addition leads to the increments of both the Si/Ba ratio and the amount of SiO_2.

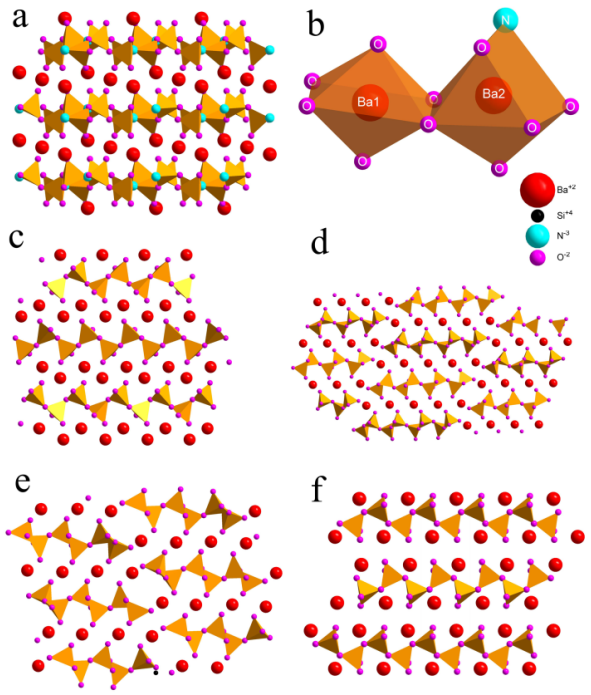

Fig. 2 Schematic crystal structure of $Ba_3Si_6O_{12}N_2$ and impurity barium orthosilicates (a: $Ba_3Si_6O_{12}N_2$ view along [010], c: $BaSi_2O_5$ view along [010], d: $Ba_5Si_8O_{21}$ view along [010], e: $Ba_4Si_6O_{16}$ view along [001] and f: $BaSiO_3$ view along [010]), and coordination polyhedra of the two difference Ba sites in $Ba_3Si_6O_{12}N_2$ (b)

Table I Ratios of Si/Ba and O/Ba in $Ba_3Si_6O_{12}N_2$ and impurity phases

Phase	Si/Ba	O/Ba
$Ba_3Si_6O_{12}N_2$	2	4
$BaSi_2O_5$	2	5
$Ba_5Si_8O_{21}$	1.6	4.2
$Ba_4Si_6O_{16}$	1.5	4
$BaSiO_3$	1	3

Figure 3 presents the excitation and emission spectra of $Ba_{2.85}Eu_{0.15}Si_6O_{12}N_2$ with varying Si/Ba ratios. As seen, the spectra show a great similarity except for the luminescence intensity, which are resulted from the same dominant phase $Ba_{2.85}Eu_{0.15}Si_6O_{12}N_2$. As the orthosilicates have no luminescence under the blue light irradiation[31, 41, 42], they only have an influence in the luminescence intensity of the phosphor. The strongest luminescence is observed when the Si/Ba is equal to 2.08.

Next, as $BaSi_2O_5$ is an oxygen-rich phase, and has a higher O/Ba ratio than $Ba_3Si_6O_{12}N_2$, the O/Ba ratio must be reduced to suppress the formation of $BaSi_2O_5$ (while keeping Si/Ba = 2.08). As shown in Fig. 4, the orthosilicate impurity phases turn to disappear with decreasing the O/Ba ratio. A phase pure $Ba_3Si_6O_{12}N_2$ is finally obtained at O/Ba = 3.52. On the other hand, another two orthosilicates ($Ba_4Si_6O_{16}$ and $BaSiO_3$) form at O/Ba ratios less than 3.4, both of which have lower Si/Ba and O/Ba ratios than $Ba_3Si_6O_{12}N_2$ (see Table I). It means that the low O/Ba ratio tends to produce $Ba_4Si_6O_{16}$ and $BaSiO_3$.

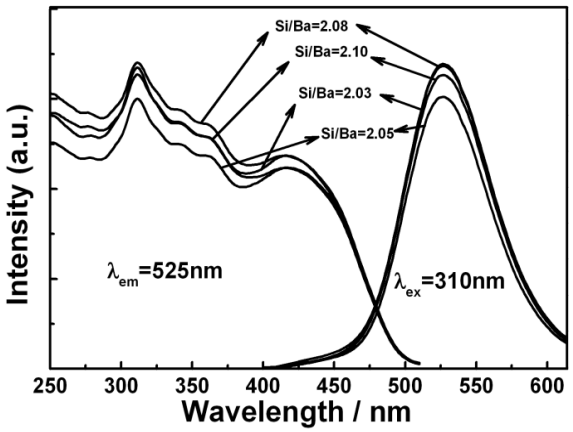

Fig. 3 Excitation (monitored at 525 nm) and emission (excited by 310 nm) spectra of $Ba_{2.85}Eu_{0.15}Si_6O_{12}N_2$ phosphors as a function of the Si/Ba ratio.

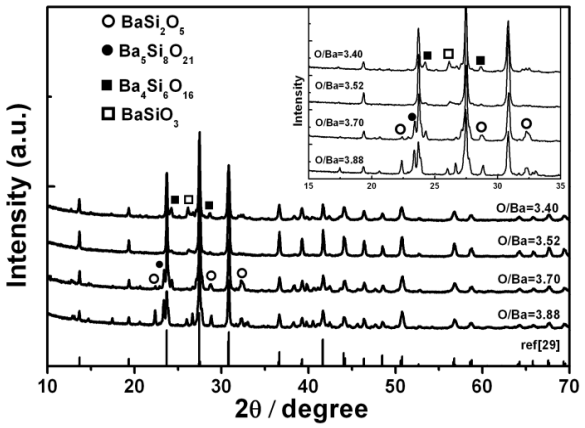

Fig. 4 X-ray diffraction patterns of $Ba_{2.85}Eu_{0.15}Si_6O_{12}N_2$ (Si/Ba = 2.08) with different ratios of O/B

As shown above, the ratios of Si/Ba and O/Ba play an important role in the formation of the pure phase of $Ba_3Si_6O_{12}N_2$. The stoichiometric ratio of Si/Ba or O/Ba in the starting materials according to $Ba_3Si_6O_{12}N_2$ cannot lead to a pure phase because the SiO_2 layer on the Si_3N_4 surface is not considered or compensated during weighing out the starting materials. $Ba_5Si_8O_{21}$ and $BaSi_2O_5$ easily form with larger Si/Ba and O/Ba ratios in the starting powders, while $Ba_4Si_6O_{16}$ and $BaSiO_3$ appear with smaller Si/Ba and O/Ba ratios. The phase pure $Ba_3Si_6O_{12}N_2$ can be achieved by the careful control of the Si/Ba (2.08) and O/Ba (3.52) ratios through increasing and decreasing the content of Si_3N_4 and SiO_2, respectively.

Figure 5 shows the XRD patterns of $Ba_{3-x}Eu_xSi_6O_{12}N_2$ (x=0.05~0.3) phosphors with Si/Ba = 2.08 and O/Ba = 3.52. The doping of Eu does not generate any other impurity phases, indicating the accommodation of Eu in the lattice of $Ba_3Si_6O_{12}N_2$.

A typical SEM image of the as-prepared Eu^{2+}-doped $Ba_3Si_6O_{12}N_2$ is shown in Fig. 6. The phosphor particles are slightly agglomerated, with the primary particle having a size of 3 μm in diameter.

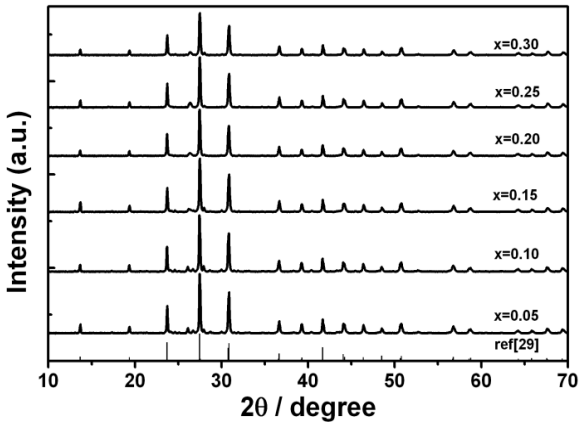

Fig. 5 X-ray diffraction patterns of $Ba_{3-x}Eu_xSi_6O_{12}N_2$ (Si/B a= 2.08 and O/Ba = 3.52)

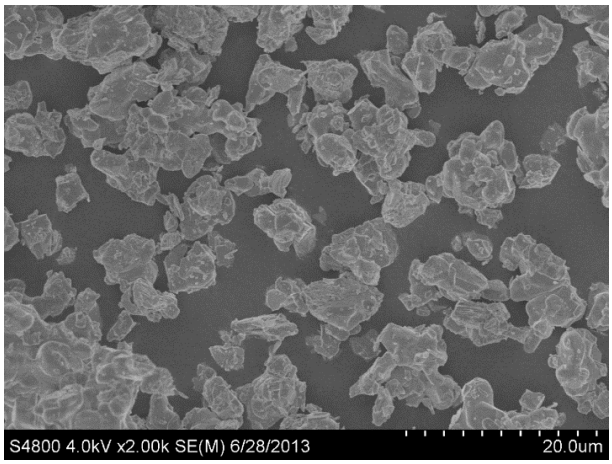

Fig. 6 SEM image of $Ba_{2.85}Eu_{0.15}Si_6O_{12}N_2$ prepared at 1350 °C

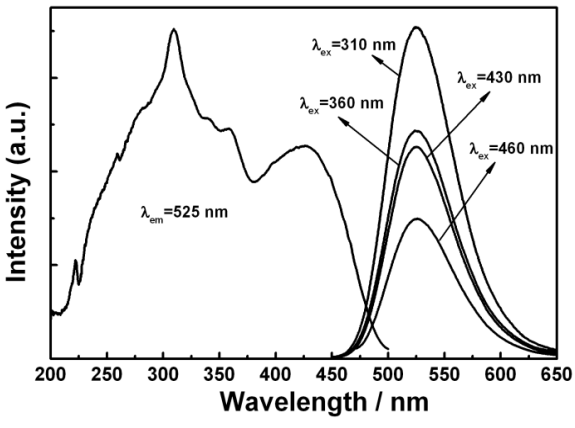

Fig. 7 Excitation (monitored at 525 nm) and emission (excited at 310, 360, 430, 460 nm) spectra of $Ba_{2.85}Eu_{0.15}Si_6O_{12}N_2$

3.2. Photoluminescence Properties

The Eu^{2+}-doped $Ba_3Si_6O_{12}N_2$ phosphor shows a very broad excitation band with the right tail extending to 500 nm, as illustrated in Fig. 7, which absorbs UV or blue light strongly and matches well with the blue LED chips. Under 310, 360, 430, or the 460 nm excitation, the emission spectra are all symmetric band centered at 525 nm, which owns to the $4f^65d^1 \rightarrow 4f^7$ transitions of Eu^{2+}. The full width at half maximum (FWHM) is about 68 nm, which is very suitable for use as a green phosphor in backlight applications.

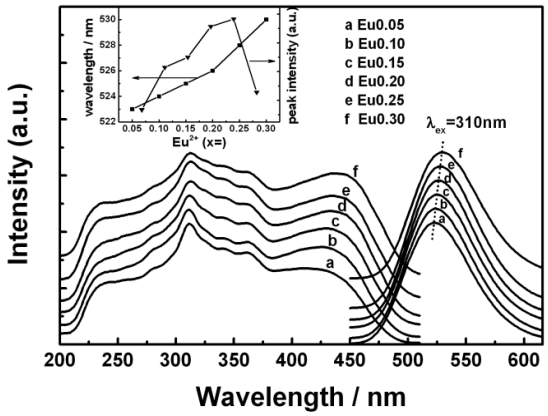

Fig. 8 Excitation (monitored at emission peak wavelength) and emission (excited at 310 nm) spectra of $Ba_{3-x}Si_6O_{12}N_2$:xEu^{2+}

As seen in Fig. 8, the concentration quenching occurs at x = 0.25 for $Ba_{3-x}Si_6O_{12}N_2$:xEu^{2+} (x = 0.05~0.3). It is mainly attributed to the energy transfer among Eu^{2+}. The probability of energy transfer is largely dependent on the distance between activator ions. With increasing the amount of doped Eu^{2+}, the distance between Eu^{2+} ions shortens, which increases the probability of nonradiative energy transfer between Eu^{2+}. As there is a small overlap between the excitation and emission spectra, the contribution of reabsorption to concentration quenching can be omitted. The critical distance for energy transfer can be roughly calculated by using Eq. (2)[43],

$$R_c = 2\left(\frac{3V}{4\pi x_c Z}\right)^{1/3} \qquad (2)$$

where x_c is the critical concentration of the activator ion, V the volume of the unit cell, and Z the cations number in the unit cell that can be occupied by activator ions. For $Ba_3Si_6O_{12}N_2$:Eu^{2+}, Braun addressed that Eu^{2+}, showed in Fig. 2, mainly occupied the Ba1 site,[30] so $Z = 1$ instead of $Z = 3$. Taking $x_c = 0.25$, $V = 316.935$ $Å^3$ into Eq. (2), the critical distance is then computed to be about *13.43 Å*.

Figure 8 also shows the redshift of the emission spectrum with increasing the Eu^{2+} concentration. When the smaller Eu^{2+} ions (r = 1.10 Å) substitute larger Ba^{2+} (r = 1.34 Å) ones, the volume lattice shrinks, resulting in a strong crystal field strength. The redshift is thus ascribed to the enhanced crystal field splitting.

3.3. *Thermal quenching*

In general, small thermal quenching is required for LED phosphors, especially those used in high-power LEDs, which can minimize the changes in chromaticity and efficiency of white LEDs. Figure 9 shows the temperature-dependent emission spectrum of $Ba_{2.85}Eu_{0.15}Si_6O_{12}N_2$. The emission spectrum is blue-shifted as the temperature is raised, which is due to the thermally induced lift up of the lowest 5d energy levels. When the phosphor is heated up to 200 ^oC, the luminescence still remains 90% of the initial intensity measured at room temperature (see Fig.10). The thermal quenching of $Ba_3Si_6O_{12}N_2:Eu^{2+}$ is much smaller than that of $Ba_2SiO_4:Eu^{2+}$ [44] and YAG:Ce^{3+} [45].

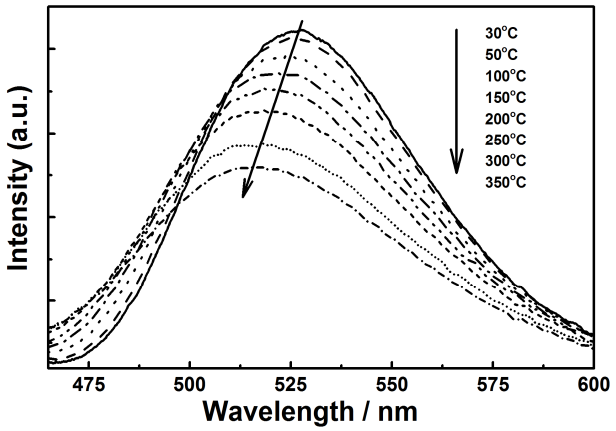

Fig. 9 The emission spectra of $Ba_{2.85}Eu_{0.15}Si_6O_{12}N_2$ (Si/Ba=2.08 and O/Ba=3.4), excited at 460 nm at varying temperatures.

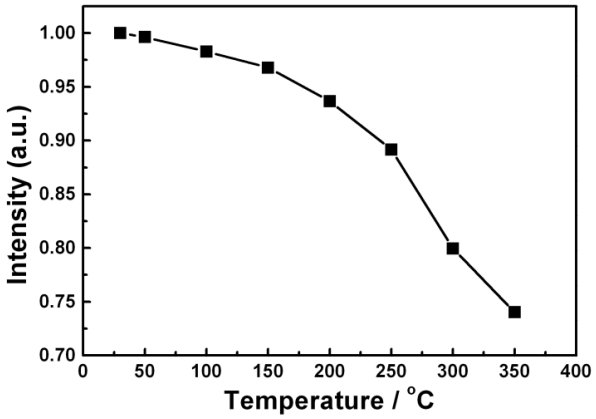

Fig. 10 Temperature dependence of the relative emission intensity for $Ba_{2.85}Eu_{0.15}Si_6O_{12}N_2$ (Si/Ba = 2.08 and O/Ba = 3.4)

Thermal quenching can be interpreted by using the configurational coordinate diagram[1, 46], as illustrated in Fig. 11. In the diagram, the X-axis represents the metal-ligand distance *R*, and the Y-axis is the energy *E* of an absorbing center. The ground state and excited state energy levels quantized for harmonic oscillator are represented by parabola U_0 and U`, respectively. A crossing point X of parabola $U_0$ and U` is indicated in the diagram, and it is at a higher energy level than point A` that is the excited state energy level of luminescent centers after being promoted by the absorbed energy. Generally, the luminescent centers go through nonradiative relaxation to the lowest vibrational level corresponding to point O`. At this moment, when temperature increases, the centers will be thermally activated from point O` to the junction point X. This means that the excited $Eu^{2+}$ ions easily reach the ground state through the phonon vibration rather than emitting photons. As a result, luminescence owing to the transition from point O` to point A is quenched. The probability of thermal quenching process is strongly dependent on the energy barrier ΔE_q between point O` and point X. A greater ΔE_q is the lower thermal quenching of the phosphor. The activation energy for thermal quenching ΔE_q can be calculated from the Arrhenius equation described by Eq. (3)[47].

$$I_T = \frac{I_0}{1 + c\exp(-\frac{\Delta E_q}{kT})} \quad (3)$$

Where I_0 is the initial emission intensity, I_T is the intensity at a given temperature *T*, *c* is a constant, and *k* is Boltzmann's constant. The ΔE_q was calculated to be 0.257eV by fitting the plot of $\ln[(I_0/I_T)-1]$ vs 1/T . The ΔE_q value for $Ba_3Si_6O_{12}N_2:Eu^{2+}$ is larger than 0.202 and 0.2 eV for Sr- and Ca-α-SiAlON:Eu^{2+} phosphors, respectively [48].

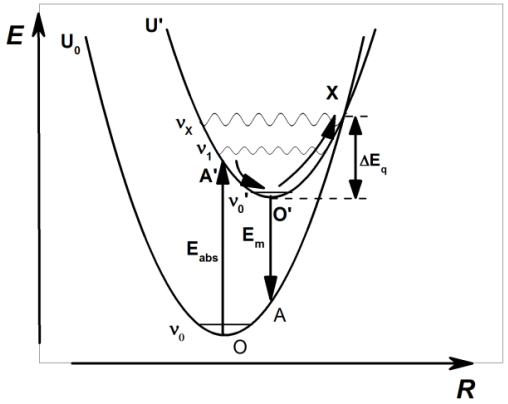

Fig. 11 Configurational coordinate diagram showing the thermal quenching process

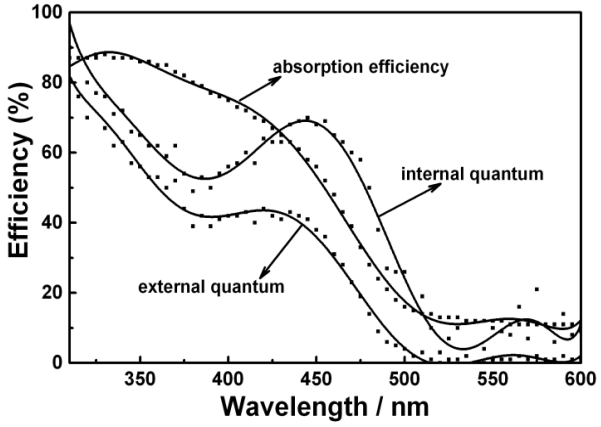

Fig. 12 Absorption, internal and external quantum efficiencies of $Ba_{3-x}Eu_xSi_6O_{12}N_2$ (x = 0.15)

3.4. Quantum Efficiency

The absorption efficiency (η_a), internal quantum efficiency (η_i) and external quantum efficiency (η_o) can be obtained by using Eqs. 4-6:[49]

$$\eta_a = \frac{\int \lambda[E(\lambda) - R(\lambda)]d\lambda}{\int \lambda E(\lambda)d\lambda} \quad (4)$$

$$\eta_i = \frac{\int \lambda P(\lambda)d\lambda}{\int \lambda[E(\lambda) - R(\lambda)]d\lambda} \quad (5)$$

$$\eta_o = \frac{\int \lambda P(\lambda)d\lambda}{\int \lambda E(\lambda)d\lambda} \quad (6)$$

where E(λ), R(λ), and P(λ) are the intensity per unit wavelength in the spectra of excitation, reflectance, and emission of the phosphor, respectively. The absorption and quantum efficiency of $Ba_{2-x}Eu_xSi_6O_{12}N_2$ (x = 0.15) as a function of the exciting wavelength are shown in Fig. 12. Under the 450 nm excitation, the absorption, internal and external quantum efficiencies of the green phosphor are 56, 68 and 38%, respectively. These data are lower than those reported by Mikami *et al.*, which could be further enhanced by optimizing the processing conditions and controlling the particle size, morphology, and crystallinity of the phosphor.

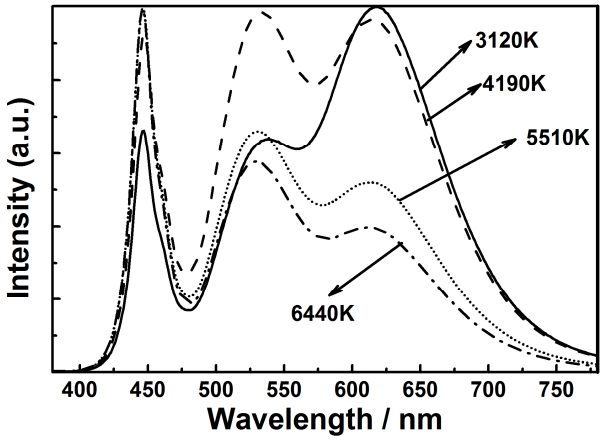

Fig. 13 Relative emission spectra of white LEDs with varying color temperatures, measured under a 20 mA drive current.

Table II Optical properties of white LEDs using $Ba_3Si_6O_{12}N_2:Eu^{2+}$

Sample	P : E	P_G: P_R	η / lm•W^{-1}	Tc / K	Ra	R9
1	0.2 : 1	93 : 7	60.6	3120	94	68
2	0.2 : 1	95 : 5	66	4190	90	61
3	0.15 : 1	95 : 5	71.8	5510	89	72
4	0.14 : 1	96 : 4	75.5	6440	88	71

3.5. LED applications

White LED lamps were prepared by combining a blue LED chip with red $Sr_2Si_5N_8:Eu^{2+}$ and green $Ba_3Si_6O_{12}N_2:Eu^{2+}$ phosphors. The emission spectra of white LEDs with varying correlated color temperatures (CCT), which are obtained by controlling the ratio of phosphors and silicone epoxy (P : G) and the ratio between green and red (P_G: P_R) phosphors, are given in Fig. 13. As seen, three primary emission bands are centered at 460 (LED chip), 530 ($Ba_3Si_6O_{12}N_2:Eu^{2+}$) and 616 nm ($Sr_2Si_5N_8:Eu^{2+}$), respectively. Three emission bands composite a spectrum that appears white to the naked eye. The optical properties of white LEDs are shown in Table II. As seen, high color rendition is obtained in this work. The average R_a values for white LEDs with varying CCT lie between 88 and 94. Moreover, the R9 values are also quite high, which is acceptable for general lighting. The average luminous efficiency (η) of the white LEDs is 60.6 ~ 75.5 lm/w, which is higher than that of cold cathode fluorescent lamps (50 lm/W, R_a=50 ~ 88)[50, 51]. This indicates that the green-emitting $Ba_3Si_6O_{12}N_2:Eu^{2+}$ phosphor is very suitable for use in high color rendering white LEDs that replace traditional fluorescent tubes or incandescent bulbs for general illumination.

Conclusions

In this work, Eu-doped $Ba_3Si_6O_{12}N_2$ green phosphors ($Ba_{3-x}Eu_xSi_6O_{12}N_2$, x = 0.05~0.3) were synthesized by the solid-state reaction at 1350℃ for 5 hours under a reducing atmosphere of N_2/H_2 (5%). The pure phase of $Ba_3Si_6O_{12}N_2$ was obtained by carefully controlling the Si/Ba and O/Ba ratios. The prepared $Ba_3Si_6O_{12}N_2:Eu^{2+}$ phosphor showed a symmetrical emission band centered at ~525 nm, and a broad excitation band covering the UV to blue light region. Compared to $Ba_2SiO_4:Eu^{2+}$ and $Y_3Al_5O_{12}:Ce^{3+}$ green phosphors, $Ba_3Si_6O_{12}N_2:Eu^{2+}$ exhibited a smaller thermal quenching. High color rendering white LEDs can be achieved by using $Ba_3Si_6O_{12}N_2:Eu^{2+}$ and a red phosphor, indicating $Ba_3Si_6O_{12}N_2:Eu^{2+}$ is a promising green phosphor for white LEDs.

Acknowledgements

This work was supported by National Natural Science Foundation of China (No. 51272259).

Notes and references

[a] Division of Functional Materials and Nanodevices, Ningbo Institute of Materials Technology and Engineering, Chinese Academy of Sciences, Ningbo, Zhejiang, 315201, China
[b] Faculty of Science, Ningbo University, Ningbo 315211, China
[c] Sialon Group, Sialon Unit, National Institute for Materials Science, Namiki 1-1, Tsukuba, Ibaraki 305-0044, Japan
† Corresponding author: E-mail: Xie.Rong-Jun@nims.go.jp; Tel: 0081-29-860-4312; Fax: 0081-29-851-3613

References

1. R.-J. Xie, Y. Q. Li, N. Hirosaki and H. Yamamoto, *Nitride Phosphors and Solid-State lighting*, Taylor & Francis, Boca Raton, 2011, pp 2-69.

2. R.-J. Xie, N. Hirosaki, K. Sakuma, Y. Yamamoto and M. Mitomo, *Appl. Phys. Lett.*, 2004, **84**, 5404.
3. M. Yamada, T. Naitou, K. Izuno, H. Tamaki, Y. Murazaki, M. Kameshima and T. Mukai, *Jpn J Appl Phys 2*, 2003, **42**, L20-L23.
4. H. S. Jang, W. B. Im, D. C. Lee, D. Y. Jeon and S. S. Kim, *J. Lumin.*, 2007, **126**, 371-377.
5. Y. Q. Li, J. E. J. van Steen, J. W. H. van Krevel, G. Botty, A. C. A. Delsing, F. J. DiSalvo, G. de With and H. T. Hintzen, *J. Alloys Compd.*, 2006, **417**, 273-279.
6. R.-J. Xie, N. Hirosaki, T. Suehiro, F.-F. Xu and M. Mitomo, *Chem. Mater.*, 2006, **18**, 5578-5583.
7. J.-M. Song, J.-S. Park and S. Nahm, *Ceram. Int.*, 2013, **39**, 2845-2850.
8. K. Uheda, N. Hirosaki, Y. Yamamoto, A. Naito, T. Nakajima and H. Yamamoto, *Electrochem Solid St*, 2006, **9**, H22-H25.
9. N. Hirosaki, R. J. Xie, K. Kimoto, T. Sekiguchi, Y. Yamamoto, T. Suehiro and M. Mitomo, *Appl. Phys. Lett.*, 2005, **86**. 211905
10. R. J. Xie, N. Hirosaki, H. L. Li, Y. Q. Li and M. Mitomo, *J. Electrochem. Soc.*, 2007, **154**, J314.
11. K. Kimoto, R.-J. Xie, Y. Matsui, K. Ishizuka and N. Hirosaki, *Appl. Phys. Lett.*, 2009, **94**, 041908.
12. J. Botterman, K. V. d. Eeckhout, A. J. J. Bos, P. Dorenbos and P. F. Smet, *Opt. Mater. Express*, 2012, **2**, 341-349.
13. V. Bachmann, T. Jüstel, A. Meijerink, C. Ronda and P. J. Schmidt, *J. Lumin.*, 2006, **121**, 441-449.
14. I. H. Cho, G. Anoop, D. W. Suh, S. J. Lee and J. S. Yoo, *Opt. Mater. Express*, 2012, **2**, 1292-1305.
15. V. Bachmann, C. Ronda, O. Oeckler, W. Schnick and A. Meijerink, *Chemistry of Materials*, 2009, **21**, 316-325.
16. O. Oeckler, J. A. Kechele, H. Koss, P. J. Schmidt and W. Schnick, *Chemistry-a European Journal*, 2009, **15**, 5311-5319.
17. R.-J. Xie, N. Hirosaki, MamoruMitomo, Y. Yamamoto, T. Suehiro and N. Ohashi, *J. Am. Ceram. Soc*, 2004, **87**, 1308-1370.
18. R.-J. Xie, N. Hirosaki, M. Mitomo, T. Suehiro, X. Xu and H. Tanaka, *J. Am. Ceram. Soc.*, 2005, **88**, 2883-2888.
19. Y. Q. Li, N. Hirosaki, R. J. Xie, T. Takeda and M. Mitomo, *Chem. Mater.*, 2008, **20**, 6704-6714.
20. L. Liu, R.-J. Xie, W. Li, N. Hirosaki, Y. Yamamoto, X. Sun and D. Johnson, *J. Am. Ceram. Soc.*, 2013, **96**, 1688-1690.
21. T. Seto, N. Kijima and N. Hirosaki, *ECS Trans.*, 2009, **25**, 247-252.
22. T. Suehiro, N. Hirosaki and R. J. Xie, *ACS Appl. Mater. Interfaces*, 2011, **3**, 811-816.
23. J. Ruan, R.-J. Xie, S. Funahashi, Y. Tanaka, T. Takeda, T. Suehiro, N. Hirosaki and Y.-Q. Li, *J. Solid State Chem.*, 2013, **208**, 50-57.
24. L. Zhang, J. Zhang, X. Zhang, Z. Hao, H. Zhao and Y. Luo, *ACS Appl. Mater. Interfaces*, 2013, DOI: 10.1039/am402612n
25. J. H. Lee and Y. J. Kim, *Mater. Sci. Eng., B*, 2008, **146**, 99-102.
26. M. A. Lim, J. K. Park, C. H. Kim, H. D. Park and M. W. Han, *J. Mater. Sci. Lett.*, 2003, **22**, 1351-1353.
27. T. E. Peters and J. A. Baglio, *J. Electrochem. Soc.*, 1972, **119**, 230-236.
28. Y. Pan, M. Wu and Q. Su, *Mater. Sci. Eng., B*, 2004, **106**, 251-256.
29. M. Mikami, S. Shimooka, K. Uheda, H. Imura and N. Kijima, *Key Eng. Mater.*, 2009, **403**, 11-14.
30. C. Braun, M. Seibald, S. L. Borger, O. Oeckler, T. D. Boyko, A. Moewes, G. Miehe, A. Tucks and W. Schnick, *Chem. Eur. J.*, 2010, **16**, 9646-9657.
31. I. Sun Cho, D. Kyun Yim, C. Hyun Kwak, J. Sul An, H. Suk Roh and K. Sun Hong, *J. Lumin.*, 2012, **132**, 375-380.
32. Y. Q. Li, A. C. A. Delsing, G. de With and H. T. Hintzen, *Chem. Mater.*, 2005, **17**, 3242-3248.
33. J. Botterman, K. V. d. Eeckhout, I. D. Baere, D. Poelman and P. F. Smet, *Acta Mater.*, 2012, **60**, 5494-5500.
34. J. A. Kechele, O. Oeckler, F. Stadler and W. Schnick, *Solid State Sci.*, 2009, **11**, 537-543.
35. H.-G. Kim, E.-H. Kang, B.-H. Kim and S.-H. Hong, *Opt. Mater.*, 2013, **35**, 1279-1282.
36. F. Stadler and W. Schnick, *Z. Anorg. Allg. Chem.*, 2006, **632**, 949-954.
37. J. Tang, J. Chen, L. Hao, X. Xu, W. Xie and Q. Li, *J. Lumin.*, 2011, **131**, 1101-1106.
38. Y. H. Song, T. Y. Choi, K. Senthil, T. Masaki and D. H. Yoon, *Mater. Lett.*, 2011, **65**, 3399-3401.
39. R. Zhang, M. Numata, T. Maeda, Y. Akazawa, K.-I. Murai and T. Moriga, *Int. J. Mod. Phys. B*, 2010, **24**, 3221-3225.
40. E. H. Kang, S. W. Choi and S. H. Hong, *ECS J. Solid State Sci. Technol.*, 2012, **1**, R11-R14.
41. K. I. Seo, J. H. Park, J. S. Kim, Y. H. Na, J. C. Choi and J. S. Bae, *Solid State Commun.*, 2009, **149**, 1578-1581.
42. S. Derenzo, G. Bizarri, R. Borade, E. Bourret-Courchesne, R. Boutchko, A. Canning, A. Chaudhry, Y. Eagleman, G. Gundiah, S. Hanrahan, M. Janecek and M. Weber, *Nucl. Instrum. Methods Phys. Res., Sect. A*, 2011, **652**, 247-250.
43. G. Blasse, *Phys. Lett. A*, 1968, **28**, 444-445.
44. I. Baginskiy, R. S. Liu, C. L. Wang, R. T. Lin and Y. J. Yao, *J. Electrochem. Soc.*, 2011, **158**, P118-P121.
45. V. Bachmann, C. Ronda and A. Meijerink, *Chem. Mater.*, 2009, **21**, 2077-2084.
46. C. C. Klick and J. H. Schulman, in *Solid State Physics*, eds. S. Frederick and T. David, Academic Press, 1957, vol. 5, pp. 97-172.
47. R.-J. Xie, N. Hirosaki, N. Kimura, K. Sakuma and M. Mitomo, *Appl. Phys. Lett.*, 2007, **90**, 191101.
48. K. Shioi, N. Hirosaki, R.-J. Xie, T. Takeda and Y. Q. Li, *J. Mater. Sci.*, 2010, **45**, 3198-3203.
49. O. Kazuaki and S. Teruaki, 1999, **83**, 87-93.
50. Y. Fukuda, K. Ishida, I. Mitsuishi and S. Nunoue, *Appl. Phys. Express*, 2009, **2**, 012401.
51. *US Pat.*, 5 838 101, 1998.

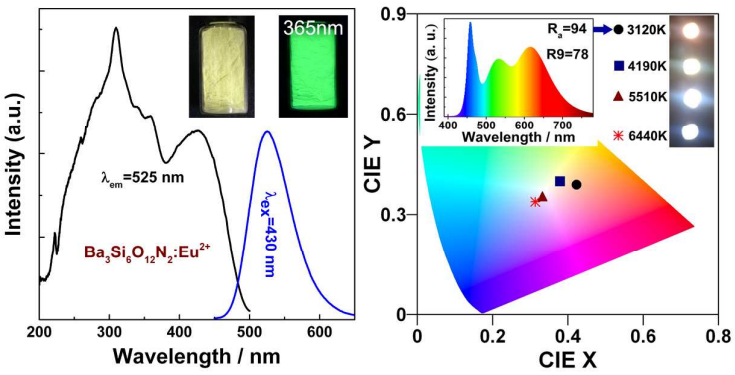

A phase pure green $Ba_3Si_6O_{12}N_2:Eu^{2+}$ phosphor (left) was successfully synthesized by controlling the Si/Ba and O/Ba of the starting materials, and it has great potentials to prepare high CRI (R_a>90) white LEDs (right).